Materials

The protonic of ZSM-22 zeolites were prepared by ion exchange to NH_4^+ form first (0.1 m NH_4NO_3, 25 °C, 3×24 h) followed by drying (100 °C, 10 h) and calcination (550 °C, 6 h).

Characterization methods

Powder X-ray diffraction (PXRD) patterns were measured in a Brucker D8 Advance operated at 40 kV and 40 mA using monochromatic Cu-Kα (λ = 1.54 Å) radiation, a scan speed of 0.5 s per step and a step size of 0.02° in 5 - 70° 2θ range. The elemental analysis of the zeolite catalysts was analyzed by inductively coupled plasma-optical emission spectrometry (ICP-OES) performed on ICP-OES Agilent 5110 instrument. Samples were digested in a solution of HF and HNO_3 and diluted with distilled water. Nitrogen physisorption isotherms were measured with a Micromeritics ASAP 2040 instrument at -196 °C. Zeolite samples were degassed at 350 °C under vacuum for 10 hours prior to physisorption measurements. The surface area was derived using the BET model. The external surface area and micropore volume were derived from constructed t-plots. Finally, the total pore volume was determined from a single point measured at $p/p_o = 0.95$. The quantification of Brønsted and Lewis acid sites (BAS and LAS, respectively) of the catalysts was investigated using Pyridine-FTIR on a Nicolet 6700 spectrophotometer operating in transmission mode. Prior to analysis, the samples were degassed at 450 ºC under vacuum for 4 h. Pyridine adsorption was performed at room temperature and after removing the physiosorbed pyridine at 150 °C, the infrared spectra were recorded. Similar operation was adopted for collidine adsorption experiment. NH_3-TPD was performed on Micromeritics ASAP 2020 instrument. Prior to measurement, the sample was pretreated under Ar gas (25 mL min^{-1}) at 550 °C for 90 min and then cooled to 100 °C. Afterward, the samples were saturated under a 3 vol% NH_3 in He flow of 25 mL min^{-1} for 1 h. Then, the flow was switched to He and kept at 120 °C for 30 min to remove physisorbed NH_3. Subsequently, NH_3 desorption was conducted up to 600 °C at a heating rate of 10 °C min^{-1} under a He flow of 25 mL min^{-1}. Transmission Electron Microscopy (TEM) micrographs were acquired using FEI® Tecnai Twin microscope in the bright

field mode, with the filament voltage set to 120 kV. For cobalt-containing zeolite, the ion-exchanging process was performed in a 0.05 M cobalt acetate solution for three times. The sample was washed thoroughly and dried at room temperature before measurement. The amounts for cobalt and aluminum are determined by ICP-OES. The relative content of paired Al and isolated Al sites were calculated as: $[Al_{(pair)}] = 2[Co]$; $[Al_{(iso)}] = [Al_{(total)}] - [Al_{(pair)}]$, where $[Al_{(pair)}]$, $[Al_{(iso)}]$, $[Al_{(total)}]$ and [Co] are the molar content of paired aluminum, isolated aluminum, total aluminum, and cobalt, respectively.

Density Functional Theory calculations.

Periodic DFT calculations were conducted using Vienna ab initio Simulation Package (VASP)[1,2], Perdew−Burke−Ernzerhof functional[3] with Grimme's dispersion correction[4] (PBE-D3), and a plane-wave basis set of the projector-augmented-wave (PAW) method[5], as successfully applied in previous studies[6,7]. An energy cut-off of 400 eV was used for the expansion of the wave function in the plane wave basis set. A (1 × 1 × 1) γ-centered k-point mesh was employed to sample the first Brillouin zone and Gaussian smearing with a width of 0.5 eV. All atoms were relaxed until electronic energies varied by $< 1 \times 10^{-5}$ eV, and the forces on all atoms were < 0.01 eV $Å^{-1}$.

Zeolite model. The TON topology of the ZSM-22 crystal model coordinates were acquired from the International Zeolite Database (IZA) with the parameters of the single unit cell used being a = 14.1050 Å, b = 17.8420 Å, c = 5.2560 Å and α = β = γ =90°. The crystal contains four unique T-sites. This study focused on the substitution of aluminum at either one (for isolated site analysis) or two (for paired site analysis) of the T1, T2, and T3 sites within the zeolite structure, with T4 being excluded as it was not accessible. The final model structure used for simulations contained 96 T-sites.

Energy analysis. The deprotonation energy was calculated from the ionic state of zeolite (heterolytic cleavage of the Bronsted proton) - ΔE_{hetero} as follows:

$$\Delta E_{hetero} = E[ZeO^-] + E[H^+] - E[ZeOH] \quad (1)$$

where, E[ZeO^-], E[ZeOH] and E[H^+] are the total energy of the zeolite anionic, protonated states of the zeolite and gas phase proton, respectively, each in their optimized geometry.

The adsorption energy (ΔE_{ads}), reaction energy (ΔE_r) and deprotonation energies are calculated as follows:

$$\Delta E_{ads} = E[\text{ZeOH+Sorbate}] - E[\text{ZeOH}] - E[\text{Sorbate}] \quad (2)$$

where, E[ZeOH], E[Sorbate] and E[ZeOH+Sorbate] are the total energy of the zeolite sorbent, the neutral gas-phase sorbate and the combined guest-host system, respectively, each in their optimized geometry. For the paired acid sites models, the parallel acid sites alignment model was used as reference. The reaction energy (ΔE_r) for a zeolite bonded moiety (acetyl) was calculated as:

$$\Delta E_r = E_{final} - E_{initial} \quad (3)$$

where, E_{final} and $E_{initial}$ are the total energy of the zeolite final and initial states, respectively, each in their optimized geometry.

Monte-Carlo calculations.

A Monte-Carlo approach was used to estimate the probability of isolated and paired framework Al atoms in TON zeolite. The crystallographic TON structure was expanded to a periodic 4 × 4 × 10 supercell and framework Al atoms were randomly distributed over tetrahedral (T) sites according to the experimental Si/Al ratio. All generated configurations satisfied Loewenstein's rule, i.e., direct Al–O–Al linkages were forbidden. For each composition, 1000 independent Al distributions were generated. Two Al atoms were considered paired when they satisfied Loewenstein's rule and were separated by ≤ 6.0 Å (minimum-image distance). The paired-Al fraction, defined as the percentage of framework Al atoms having at least one acceptable partner, was averaged over 1000 independent Monte Carlo configurations. To assess the effect of steric accessibility, a 2.0 Å spherical probe, representing a simplified partially hydrated Co^{2+} species, was used to identify the subset of paired Al lining the same channel and thus accessible within the TON

pore network. Under these conditions, the fraction of accessible paired Al atoms was 24%. This value is comparable to the experimentally determined Co-exchangeable Al fraction (19%). Because the calculated value depends on the assumed Al–Al cutoff and probe size, this is best read as broad consistency rather than quantitative confirmation.

Catalytic tests

Catalytic experiments for ethylene oligomerization were performed in a four channel Flowrence® XD from Avantium.[8] Prior to the reaction, zeolites were pelletized and crushed into 150-250 μm particles and the obtained catalysts were mixed with SiC with a ratio of 1:6 (catalyst:SiC). Then, the catalytic bed was pretreated with N_2 at 550 °C for 2 h. Reaction temperatures from 350 to 425 °C were tested and the *WHSV* value of methanol was 5 h^{-1}, with ethylene being diluted in N_2 to a constant molar ratio of 1:1 at ambient pressure. The reaction products were analyzed on line by means of gas chromatography (GC) in an Agilent 7890B with three detectors: 2 FIDs and 1 TCD. The TCD channel has a PPQ as a backflush column, a Hayesep Q column for separation of CO_2 and a Molsieve as an analytical column for the separation of He, H_2, N_2, CH_4 and CO. All other compounds (water, hydrocarbons and oxygenates) are backflushed. The FID is equipped with a 10-m precolumn with a wax stationary phase. The separation of C_1-C_5 hydrocarbons is carried out on a 30-m Gaspro stationary phase. And the separation of methanol and aromatics is carried out on a 30-m Wax stationary phase.

Ethene conversion (X, %), and selectivity (S, %) of each *i* product are defined as follows:

$$X = \frac{C_{Ethene_{in}} - C_{Ethene_{out}}}{C_{Ethene_{in}}} \times 100 \qquad \textit{Equation 1}$$

$$S_i = \frac{i \times C_i}{2C_{Ethene_{in}} - 2C_{Ethene_{out}}} \times 100 \qquad \textit{Equation 2}$$

where $C_{Ethene_{in}}$, and $C_{Ethene_{out}}$ are the concentrations determined by GC analysis of ethene in the blank, and in the reactor effluent, respectively.

Turnover frequency (TOF) is defined as follows:

$$TOF = \frac{X \times n_{ethene}}{C_{acid} \times m_{catalyst}} \qquad \textit{Equation 3}$$

where X, n_{ethene}, C_{acid} and $m_{catalyst}$ are the conversion of ethene, the molar flow rate of ethylene, the concentration of BAS, and the mass of catalyst, respectively.

Table S1. Derived parameters from N_2 physisorption isotherms.

Sample	**S_{BET}[a] (m^2/g)**	**S_{ext}[b] (m^2/g)**	**V_{micro}[b] (cm^3/g)**	**V_{tot}[c] (cm^3/g)**
HZ-25(19%)	161	52	0.05	0.20
HZ-27(10%)	167	56	0.05	0.20
HZ-34(17%)	219	44	0.05	0.19
HZ-35(12%)	212	87	0.06	0.26

Note: [a] Derived from the BET model. [b] Derived from the t-plot method. [c] Derived from single point at p/p_0 = 0.95. S_{BET}, S_{ext}, V_{tot} and V_{micro} represent the surface area, the external surface area, the total pore volume and the micropore volume, respectively.

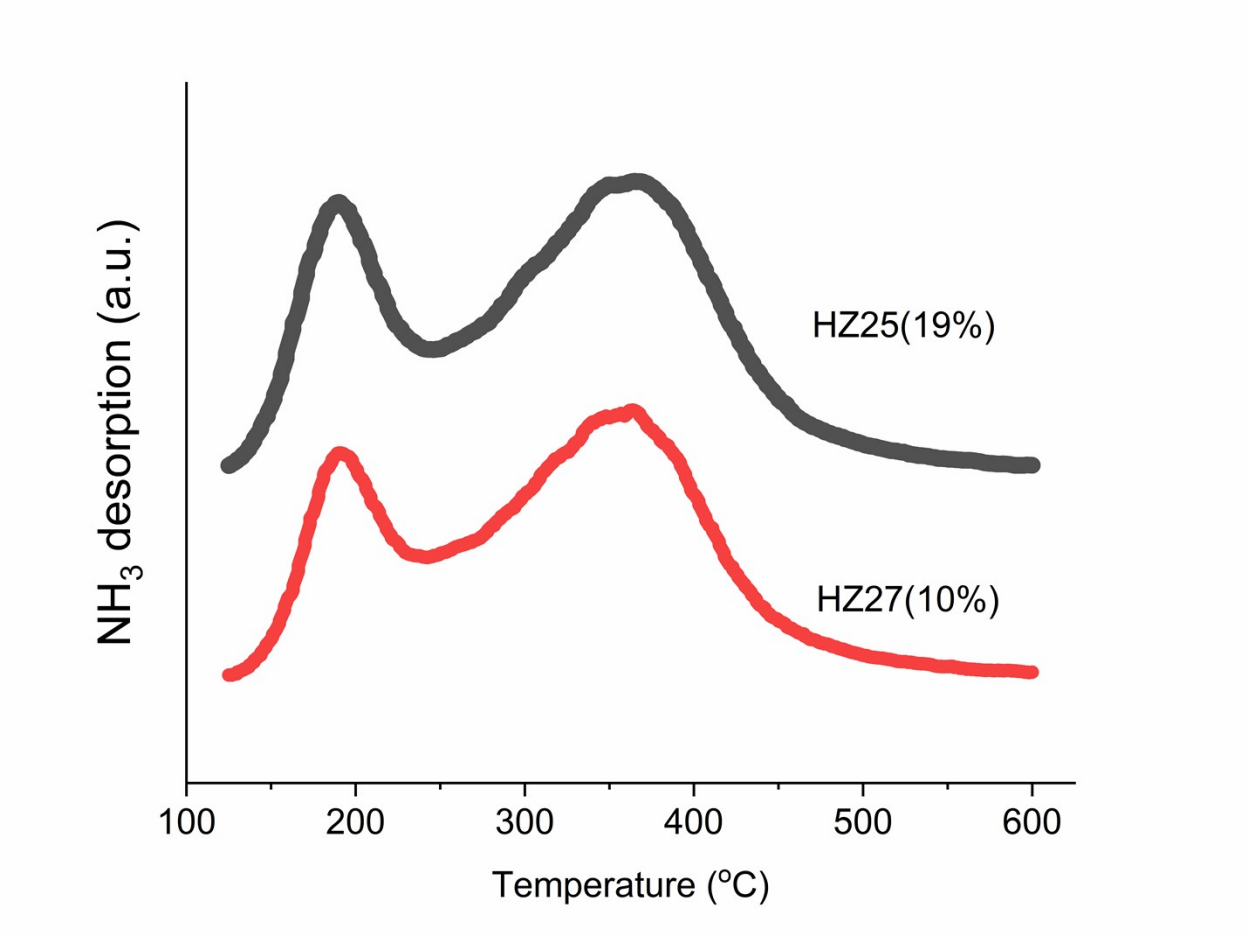

Fig. S1. NH_3-TPD profiles. The NH_3-TPD profiles display two desorption peaks, i.e., the low-temperature one situated below 250 °C and the high-temperature one located above 250 °C, which are ascribed to ammonia adsorbed on the weak and strong acid sites, respectively. The concentration of acid sites for HZ-25(19%) and HZ-27(10%) are comparable (460 vs 409 μmol g^{-1}). Moreover, similar evolutions were observed, suggesting that their acid sites distributed across the acidic strength are very similar.

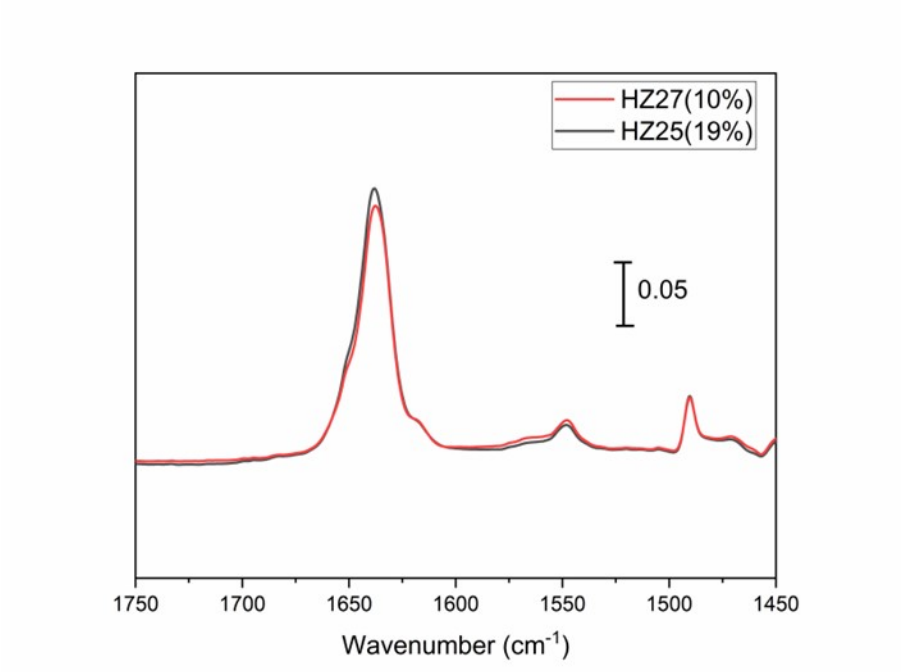

Fig. S2. FT-IR spectra after collidine adsorption. Using collidine as probe molecule, we characterized the external surface BAS for HZ-25(19%) and HZ-27(10%). As displayed, the band centered at 1638 cm^{-1} is attributed to the protonated collidinium ion over BAS. From the band intensities, these two samples do not differ much in the concentration of external surface acid sites.

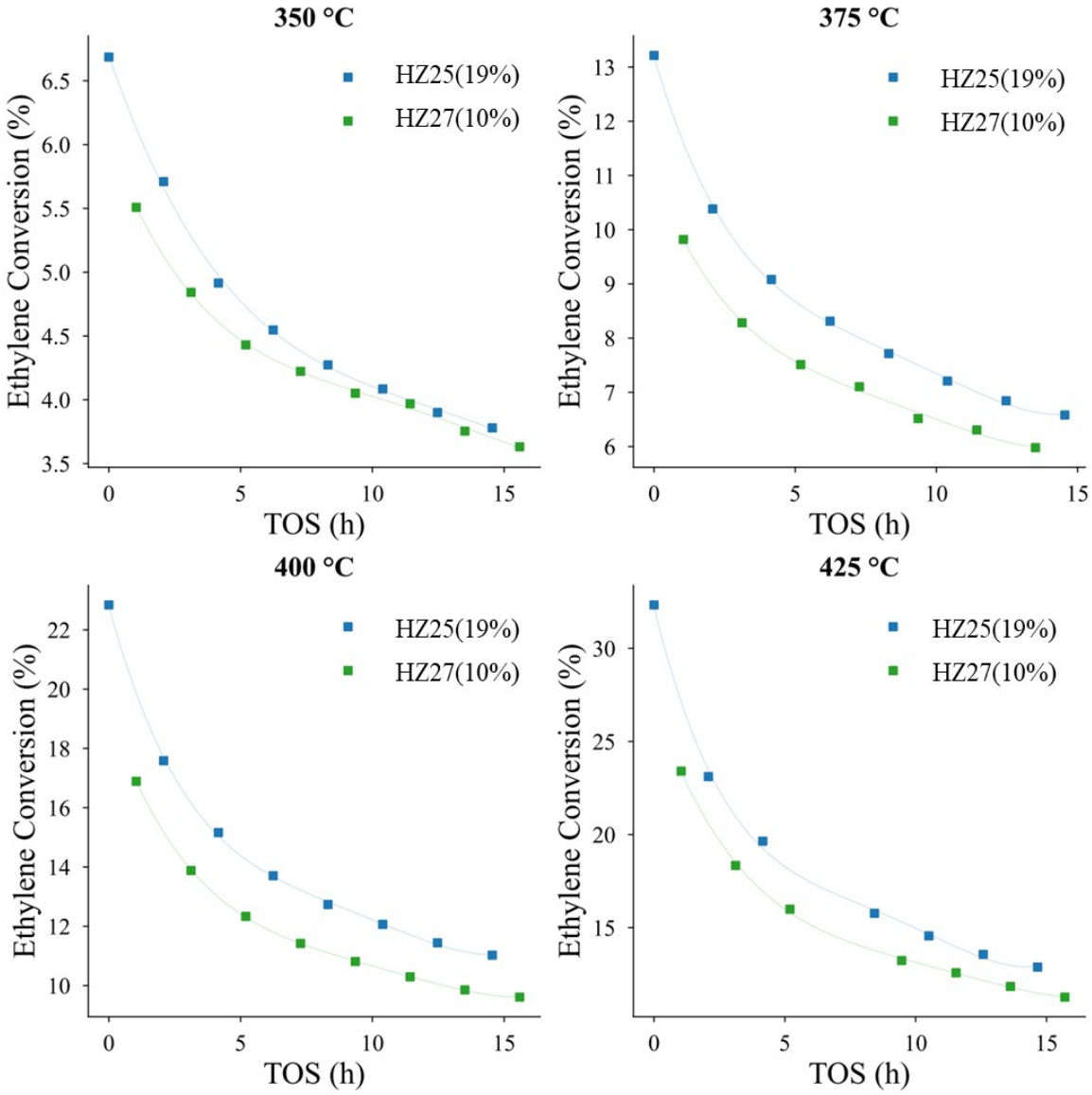

Fig. S3. Conversion of ethylene at different temperatures.

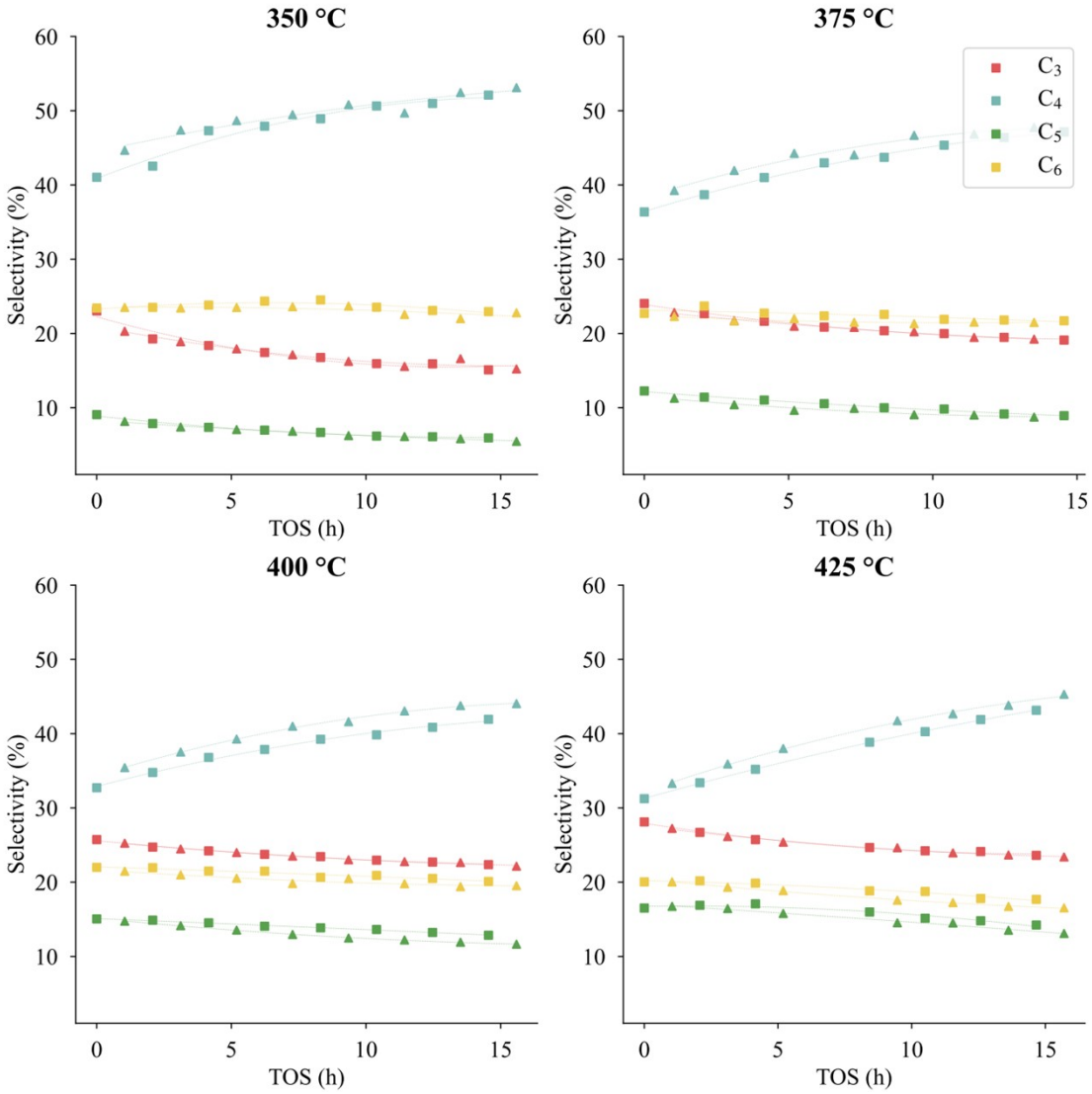

Fig. S4. Product selectivities at different temperatures. Cube: HZ25(19%); triangle: HZ27(10%).

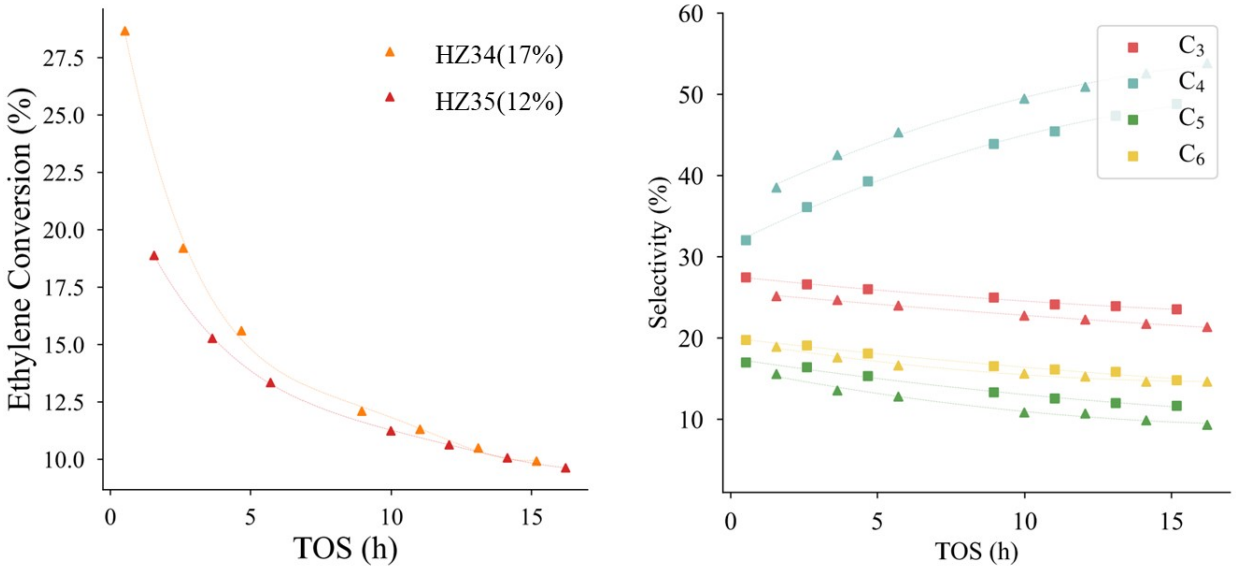

Fig. S5. Catalytic performance of HZ34(17%) and HZ35(12%) at 425 °C.

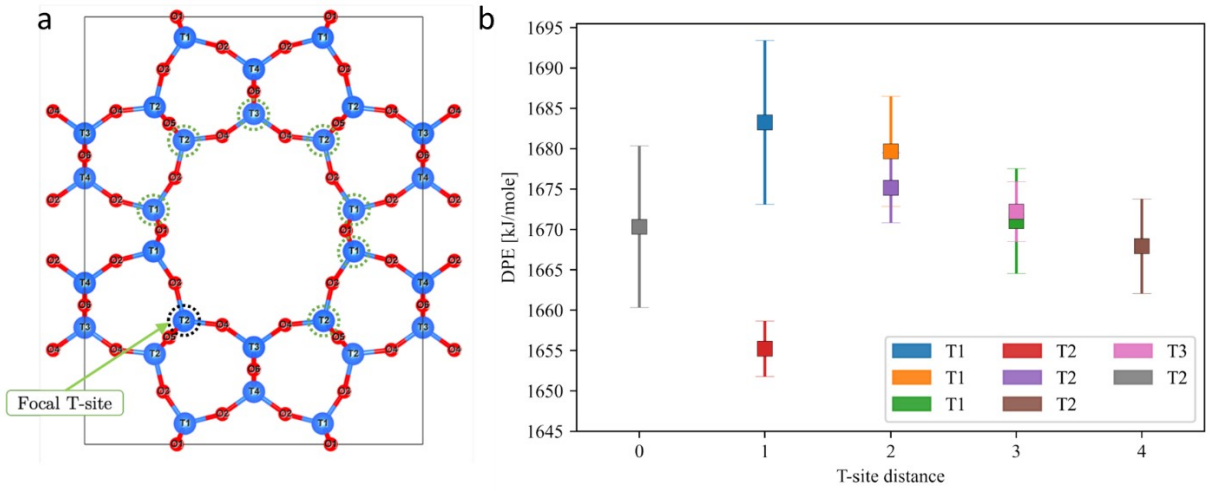

Fig. S6. (a) The models used for paired DPE calculations. T2 is chosen as a focal T-site as circled by black dash line, and its paired site used for replacing Si with an Al was circled by green dash line. (b) The deprotonation energies of isolated T2 (T-site distance = 0) compared to paired sites. Each color corresponds to the substitution position of the neighboring heteroatom.

References

1. Kresse, G., and Furthmüller, J. (1996). Efficiency of ab-initio total energy calculations for metals and semiconductors using a plane-wave basis set. Computational materials science *6*, 15-50.
2. Kresse, G., and Hafner, J. (1994). Ab initio molecular-dynamics simulation of the liquid-metal–amorphous-semiconductor transition in germanium. Physical Review B *49*, 14251.
3. Perdew, J.P., Burke, K., and Ernzerhof, M. (1996). Generalized gradient approximation made simple. Physical review letters *77*, 3865.
4. Grimme, S., Antony, J., Ehrlich, S., and Krieg, H. (2010). A consistent and accurate ab initio parametrization of density functional dispersion correction (DFT-D) for the 94 elements H-Pu. The Journal of chemical physics *132*, 154104.
5. Kresse, G., and Joubert, D. (1999). From ultrasoft pseudopotentials to the projector augmented-wave method. Physical review b *59*, 1758.
6. Ramirez, A., Gong, X., Caglayan, M., Nastase, S.-A.F., Abou-Hamad, E., Gevers, L., Cavallo, L., Dutta Chowdhury, A., and Gascon, J. (2021). Selectivity descriptors for the direct hydrogenation of CO2 to hydrocarbons during zeolite-mediated bifunctional catalysis. Nature communications *12*, 1-13.
7. Cnudde, P., De Wispelaere, K., Van der Mynsbrugge, J., Waroquier, M., and Van Speybroeck, V. (2017). Effect of temperature and branching on the nature and stability of alkene cracking intermediates in H-ZSM-5. Journal of Catalysis *345*, 53-69.
8. Shoinkhorova, T., Cordero-Lanzac, T., Ramirez, A., Chung, S.-h., Dokania, A., Ruiz-Martinez, J., and Gascon, J. (2021). Highly selective and stable production of aromatics via high-pressure methanol conversion. ACS Catalysis *11*, 3602-3613.